Int J Adv Manuf Technol (2013) 64:1737–1749
DOI 10.1007/s00170-012-4137-9

ORIGINAL ARTICLE

Cutting forces, chip formation, and tool wear in high-speed face milling of AISI H13 steel with CBN tools

Xiaobin Cui · Jun Zhao · Xianhua Tian

Received: 25 November 2011 / Accepted: 4 April 2012 / Published online: 28 April 2012

Abstract High-speed face milling experiments of AISI H13 steel (46–47 HRC) with cubic boron nitride (CBN) tools were conducted in order to identify the characteristics of cutting forces, chip formation, and tool wear in a wide range of cutting speed (200–1,200 m/min). The velocity effects are focused on in the present study. It was found that, at the cutting speed of 800 m/min, which can be considered as a critical value, relatively low mechanical load, relatively low degree of chip segmentation, and relatively long tool life can be obtained at the same time. Both the cutting forces and the degree of chip segmentation firstly decrease and then increase with the cutting speed, while the tool life exhibits the opposite trend. By means of analyzing the wear mechanisms of tools tested under different cutting speeds, it was found that, as the cutting speed increases, the influences of fracture and chipping resulting from mechanical load on tool wear were reduced, while the influences of adhesion, oxidation, and thermal crack accelerated by high cutting temperature became greater. There exist obvious correlations among cutting forces, chip formation, and tool wear.

Keywords Cutting forces · Chip formation · Tool wear · High-speed face milling · CBN tool

1 Introduction

With the development of rigid machine tools and hard cutting materials, the technology of high-speed machining has been widely applied in the field of manufacturing components in their hardened state.

Due to the retention of strength to higher temperatures than other tool materials, excellent abrasion resistance, and resistance to reaction with the ferrous work materials, the cubic boron nitride (CBN) tool material is preferred for the machining of hardened steel [1]. There have been considerable amounts of research [2–8] on cutting forces and surface roughness in turning hardened steels with CBN tools. Many studies [9–15] have also been conducted in order to investigate CBN tool wear in hard turning. These works provide much valuable information for the application of CBN tools in hard turning theoretically and experimentally.

However, relatively scant researches have been conducted in the field of milling hardened steel with CBN tools. Aslan [16] studied the performance and wear behavior of different cutting tools in end milling of X210 Cr12 cold work tool steel (62 HRC). When CBN tools were used, the best cutting performance can be reached in terms of flank wear and surface finish. End milling of AISI D2 hardened steel (58 HRC) with a round CBN insert used was conducted by Koshy et al. [17]. Acceptable tool life and good surface finish can be obtained. Fracture of the cutting edge was the governing wear mechanism for CBN tools. Braghini and Coelho [18] presented a study of the wear of CBN and cemented carbide tools in end milling AISI D6 hardened steel (58 HRC) at low/medium cutting speeds. It was found that the CBN tools could produce R_a values in the range of those obtained with surface grinding. The main wear mechanism of the CBN tools was a combination of adhesion and abrasion. Okada et al. [19] investigated the cutting performance of CBN tools and PVD-coated carbide tools in end milling of hardened steel. Tool wear, tool flank temperature, cutting force, and surface roughness were studied practically. The results showed that the CBN tools and coated

X. Cui · J. Zhao (✉) · X. Tian
Key Laboratory of High Efficiency and Clean Mechanical Manufacture of MOE, School of Mechanical Engineering, Shandong University,
Jinan 250061, People's Republic of China
e-mail: zhaojun@sdu.edu.cn

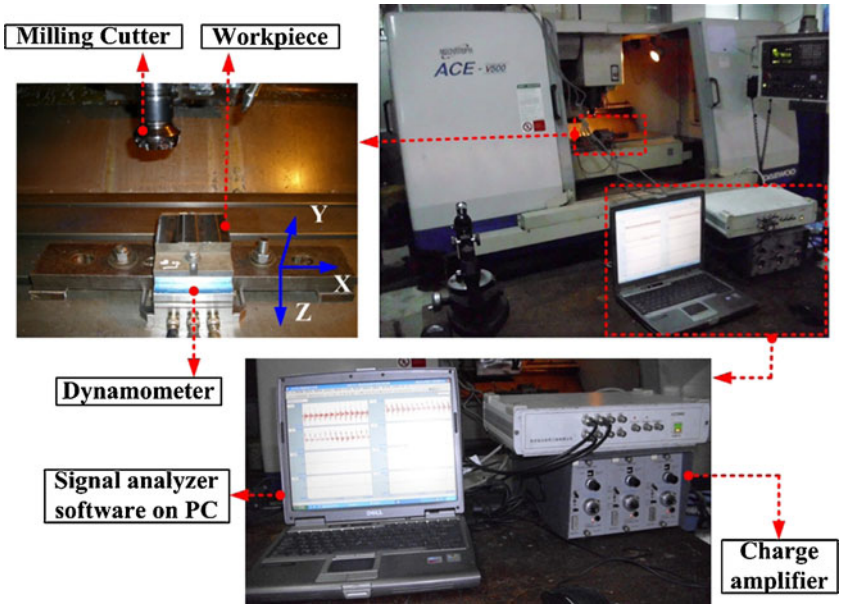

Fig. 1 The experimental setup of face milling tests

carbide tools such as coated TiAlN and TiAlN/AlCrN could adequately be applied to high- and low-speed hardmilling, respectively. It can be concluded that these previous studies mainly focus on cutting performance and tool wear in end milling. Very few studies were conducted in the field of face milling of hardened steel. Studies on cutting forces and chip formation, both of which have great effect on cutting performance and tool wear, are very scant. In these researches, the cutting speeds adopted were limited to be no more than 600 m/min.

In the present study, high-speed face milling experiments of AISI H13 steel (46–47 HRC) are performed with CBN tools used. High cutting speeds over a wide range (200–1,200 m/min) are applied. The velocity effects on cutting forces, chip formation, and tool wear are concentrated on. The variation trends of cutting forces and chip formation with cutting speed are analyzed so as to identify the characteristics of mechanical load, mechanical impact, and thermal impact. Based on the analysis results, the CBN tool wear mechanisms in high-speed face milling are revealed.

2 Experimental procedures

2.1 Cutting tool and machine tool

CBN inserts SNGN 090308S-01020 CBN100 made and recommended by Seco Tool Company were used in the milling tests. The CBN insert had negative chamfer angle which was beneficial for protecting the tool from chipping. Seco R220.74-0063-09-6 tool holder with a tool diameter of 63 mm was adopted. Taking the mechanical and thermal impact in the milling process into account, a relatively large major cutting edge angle of 75 ° was adopted. Mainly due to the high brittleness and low fracture toughness of the CBN tool, the axial rake angle (−6 °) and radial rake angle (−7 °) were designed to be negative. The tool holder is capable of carrying six inserts. Only one of the teeth was used in all the milling tests so as to avoid the effect of small difference between the teeth and maintain constant cutting conditions. All the milling tests were conducted under dry condition on a vertical CNC machining center DAEWOO ACE-V500 with a maximum spindle rotational speed of 10,000 rpm and a 15-kW drive motor as shown in Fig. 1.

2.2 Workpiece material

Because of its great high-temperature strength and wear resistance, AISI H13 tool steel is widely applied in extrusion, hot forging, and pressure die casting. In the present study, a block of AISI H13 hardened steel was used. The hardness test showed that the workpiece was hardened to 46 to 47 HRC. The width and length of the workpiece block are 75 and 100 mm, respectively. The actual chemical composition of the workpiece was tested prior to the cutting tests, and the results showed that it was consistent with the nominal chemical composition of the AISI H13 tool steel as shown in Table 1.

Table 1 Nominal chemical composition of AISI H13 tool steel (wt.%)

C	Mn	Si	Cr	Mo	V	Ni	Fe
0.32–0.45	0.20–0.50	0.80–1.2	4.75–5.50	1.10–1.75	0.80–1.20	0–0.30	Bal.

Table 2 Cutting parameter combinations adopted in the milling tests

Exp. no.	v (m/min)	f_z (mm/tooth)	a_p (mm)
1	400	0.05	0.30
2	400	0.10	0.30
3	400	0.15	0.30
4	400	0.10	0.15
5	400	0.10	0.30
6	400	0.10	0.45
7	1,200	0.05	0.30
8	1,200	0.10	0.30
9	1,200	0.15	0.30
10	1,200	0.10	0.15
11	1,200	0.10	0.30
12	1,200	0.10	0.45

2.3 Cutting tests

As recommended by the tool supplier, up-milling was adopted. Radial depth of cut a_e was set as invariable 31.5 mm. The influences of cutting speed v on cutting forces, chip formation, and tool wear are focused on.

Firstly, experiments with cutting speed ranging from 200 to 1,200 m/min with 100 m/min as an interval were performed. Feed per tooth f_z and axial depth of cut a_p were fixed as 0.1 mm/tooth and 0.3 mm, respectively. After that, tests under cutting parameter combinations listed in Table 2 were conducted in order to identify the differences of the effects of feed per tooth and axial depth of cut on cutting forces in different cutting speed ranges.

Each test was replicated three times under given milling conditions. The cutting forces were measured by means of Kistler piezoelectric dynamometer (type 9257A) mounted on the machine table as shown in Fig. 1. Before the milling tests, it was calibrated both statically and dynamically. The charge generated at the dynamometer was amplified using a multi-channel charge amplifier. The force sensor output was filtered to eliminate high-frequency noise caused by the process variables. The sampling frequency of data was set to be 4,000 Hz. During the milling tests, the flank wear values of the cutting tools were examined periodically with an optical microscope. Tool life was recorded when the flank wear reached or increased over 0.3 mm. After the experiments, the chips and worn tools were observed using a Keyence VHX-600E 3D digital microscope and scanning electron microscopy (SEM). The worn tools were also analyzed by means of energy dispersive X-ray spectroscopy (EDS).

3 Results and discussion

3.1 Cutting forces

During the first pass of the workpiece surface, the cutting forces were recorded when the milling cutter reached the

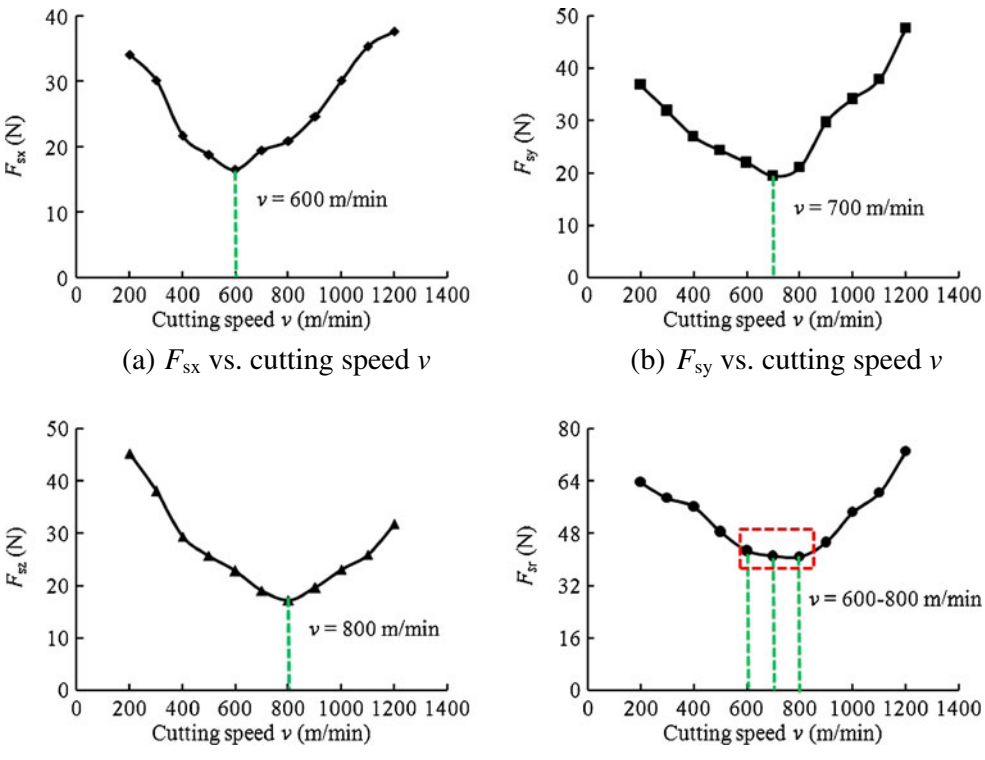

(a) F_{sx} vs. cutting speed v (b) F_{sy} vs. cutting speed v

(c) F_{sz} vs. cutting speed v (d) F_{sr} vs. cutting speed v

Fig. 2 The evolution of cutting forces with cutting speed v (f_z=0.1 mm/tooth, a_p=0.3 mm). **a** F_{sx} vs. cutting speed v, **b** F_{sy} vs. cutting speed v, **c** F_{sz} vs. cutting speed v, **d** F_{sr} vs. cutting speed v

midpoint of the workpiece. There were 4,000 data points in each recorded signature per cutting force component. The data points of the resultant cutting force F_{ri} are calculated as shown in Eq. (1):

$$F_{ri} = \sqrt{F_{xi}^2 + F_{yi}^2 + F_{zi}^2} \quad (1)$$

where F_{xi}, F_{yi}, and F_{zi} are data points of the cutting forces in X, Y, and Z directions, respectively. Taking the continuous variability of the sampled data into account, the static force component F_s in certain direction can be defined as the mean value of the corresponding sampled data point F_i [20] as shown in Eq. (2):

$$F_s = \frac{1}{N}\left(\sum_{i=1}^{N} F_i\right) \quad (2)$$

where N is the number of data points. F_{sx}, F_{sy}, and F_{sz} are used to represent the static cutting force in X, Y, and Z directions, respectively. F_{sr} is the static component of the resultant cutting force.

Figure 2 shows the evolution of the cutting forces with cutting speed. It can be seen that all the cutting forces exhibit similar developing trends. They all firstly decrease with the cutting speed and reach a valley value. Then, they increase with cutting speed. The cutting forces F_{sx}, F_{sy}, and F_{sz} arrive at valley values at cutting speeds of 600, 700, and 800 m/min, respectively. When the cutting speed is between 600 and 800 m/min, the resultant cutting force F_{sr} is relatively lower. It was found that, when 800 m/min is adopted, the smallest value of F_{sr} appears. The cutting speed of 800 m/min can be considered as a critical cutting speed at which low mechanical load can be obtained.

As the cutting speed increases, higher temperature generates in the shear zone, leading to great reduction in shear strength of the workpiece material in the shear zone [21]. When the cutting speed is high, with the increase of cutting speed, the friction between the tool rake face and the chip will be reduced because of the increase of cutting temperature [22]. An increase in cutting speed would also lead to an

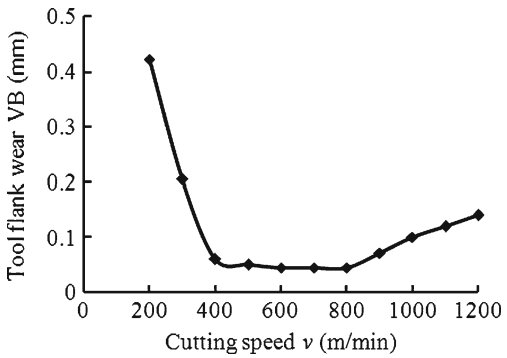

Fig. 3 Tool flank wear VB after one pass of the workpiece surface vs. cutting speed v (f_z =0.1 mm/tooth, a_p=0.3 mm)

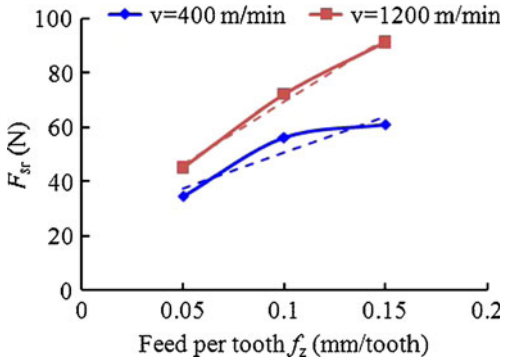

Fig. 4 The resultant cutting force F_{sr} vs. feed per tooth f_z (a_p=0.3 mm)

increase in the shear plane angle and a corresponding reduction in chip thickness and tool–chip contact area [23]. Due to the combined effects of these influencing factors, the cutting forces initially decrease with the cutting speed as shown in Fig. 2. Figure 3 shows the tool flank wear after one pass of the workpiece surface. Probably due to the effect of the mutual interaction between the cutting forces and tool wear, both of them exhibit similar evolving trends with the cutting speed. When the cutting speed is relatively low, the relatively high mechanical load makes the tools more inclined to wear, which subsequently results in the increase of cutting forces. This is more obvious when the cutting speed is below 400 m/min.

Figure 3 shows that, as the cutting speed increases over 800 m/min, the tool flank wear increases rapidly with the cutting speed. When higher cutting speed is adopted, the effect of the higher cutting temperature on tool wear will be significant. Thermal crack, fiercer diffusion, oxidation, and adhesion probably will happen on the tool. The higher tool wear rate has a greater effect on cutting forces than the higher cutting temperature does, leading to the increasing trend of the cutting forces as shown in Fig. 2.

As has been discussed, when the cutting speed of 800 m/min is adopted, the lowest mechanical load can be obtained. Two cutting speeds, 400 and 1,200 m/min, were chosen to identify the differences in the effects of feed per tooth and depth of cut on the resultant cutting force F_{sr} in different

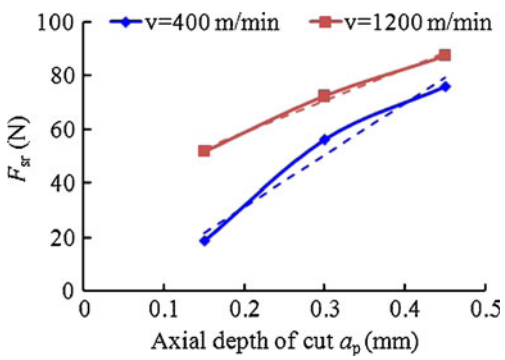

Fig. 5 The resultant cutting force F_{sr} vs. depth of cut a_p (f_z =0.1 mm/tooth)

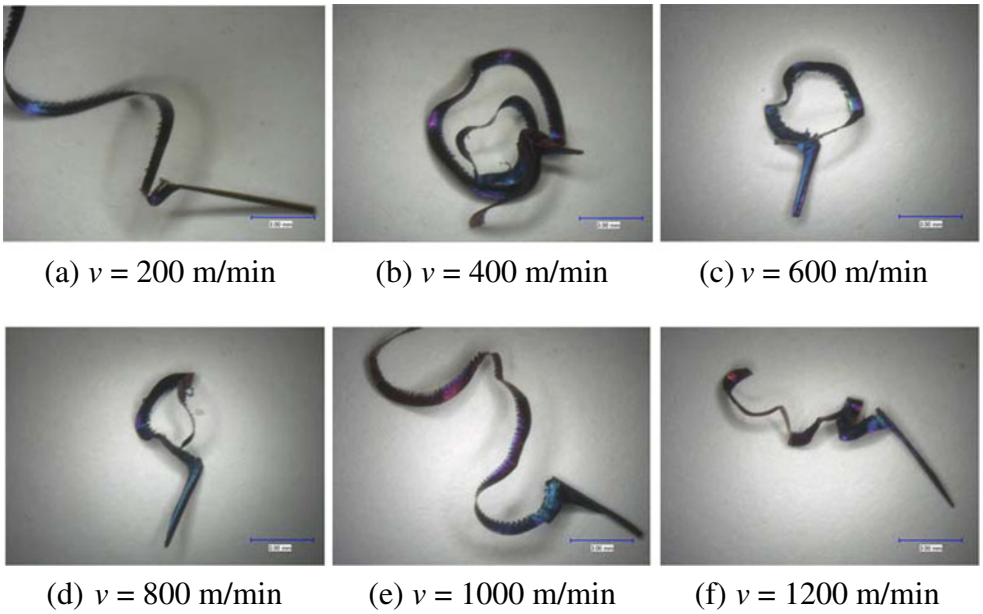

Fig. 6 Chip morphologies obtained under different cutting speeds (f_z =0.1 mm/tooth, a_p= 0.3 mm). **a** v=200 m/min, **b** v= 400 m/min, **c** v=600 m/min, **d** v=800 m/min, **e** v=1,000 m/ min, **f** v=1,200 m/min

cutting speed ranges (< 800 and ≥ 800 m/min). The cutting parameter combinations adopted are shown in Table 2. Figures 4 and 5 show the evolutions of F_{sr} with feed per tooth and depth of cut. The fitted straight lines of the curves are also shown in Figs. 4 and 5. By comparing the slopes of the fitted straight lines, it was found that, as the cutting speed increases over 800 m/min, the influence of feed per tooth f_z and axial depth of cut a_p on F_{sr} increases and decreases, respectively.

3.2 Chip formation

Figure 6 shows the chip morphologies obtained under different cutting speeds. It can be seen that, as the cutting speed increases, the shape of the chip evolves in a regular way: long helix chip (v=200 m/min), washer-shaped chip (v= 400 m/min), short arc-shaped chip (v=600 m/min, v= 800 m/min), long helix chip (v=1,000 m/min, v=1,200 m/ min). It should be pointed out that, compared with the chip

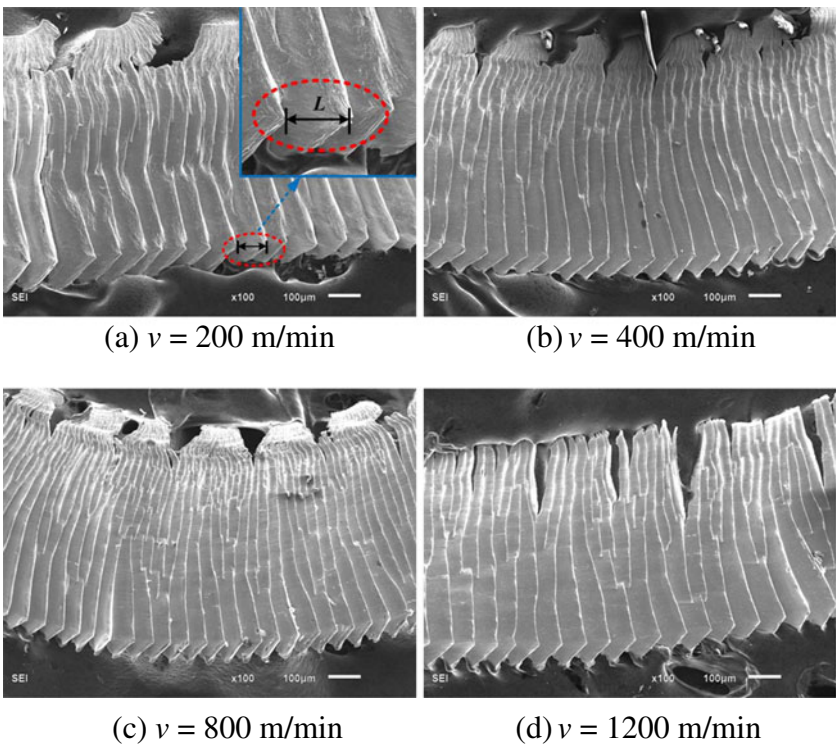

Fig. 7 Magnified chip morphologies obtained under different cutting speeds (f_z= 0.1 mm/tooth, a_p=0.3 mm). **a** v=200 m/min, **b** v=400 m/min, **c** v=800 m/min, **d** v=1,200 m/min

obtained under a cutting speed of 200 m/min, the long helix chip at 1,000 and 1,200 m/min, respectively, is curlier. This can be attributed to the higher cutting temperature under which the chip is more inclined to be distorted. The short arc-shaped chip indicates that, when the cutting speed is between 600 and 800 m/min, chip breaking is more likely to happen.

Figure 7 shows the typical magnified chip morphologies obtained under four cutting speeds. The magnified areas are all located in the middle part of the corresponding chips. The length between the sawtooth segment tips is denoted as L as shown in Fig. 7a. The length L is used to reflect the degree of segmentation. For the chip obtained under each combination of cutting parameter, this length is measured five times and the average value is calculated. The development of length L with cutting speed is shown in Fig. 8. It was found that, as the cutting speed increases, L initially decreases with the cutting speed, and when the cutting speed is above 800 m/min, it keeps increasing.

As is stated by Ai [22], due to the increase of strain rate, the increase of cutting speed will cause the enhancement of brittleness of the workpiece material, leading to a higher tendency of forming serrated chip, while the higher cutting temperature that resulted from higher cutting speed will reduce the brittleness. When the cutting speed is relatively low, the reduction of brittleness caused by the low cutting temperature is little. Though the strain rate is relatively small, the length L is still large. As the cutting speed increases, both the cutting temperature and strain rate increase. Probably due to the greater effect of cutting temperature, L decreases with the cutting speed when it is below 800 m/min. It seems that, at the cutting speed of about 800 m/min, the effects of strain rate and cutting temperature reach a balance. When the cutting speed increases over 800 m/min, the effect of strain rate on the formation of serrated chip is greater than that of cutting temperature, leading to the increasing trend of length L.

The formation of chip is a process during which the tool and workpiece material keep interacting with each other. The larger value of length L indicates that, when the cutting speed is relatively low or high, the mechanical and thermal impacts acting on the cutting tool are fiercer during the formation of each sawtooth. This is harmful to the cutting tool. Taking the evolution of the resultant cutting force shown in Fig. 2d into consideration, it is reasonable to speculate that, when the cutting speed is close to 800 m/min, relatively long tool life is expected to be obtained.

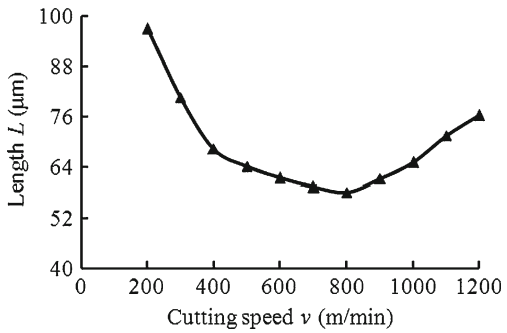

Fig. 8 The development of length L with cutting speed v (f_z=0.1 mm/tooth, a_p=0.3 mm)

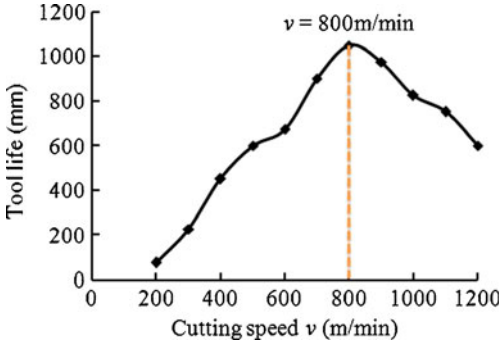

Fig. 9 Tool life vs. cutting speed v. (f_z=0.1 mm/tooth, a_p=0.3 mm)

3.3 Tool wear

In the present study, tool life is represented by feed length. As is shown in Fig. 9, when the cutting speed is no more than 800 m/min, the tool life increases with cutting speed and reaches a peak value at the cutting speed of 800 m/min. When the cutting speed is above 800 m/min, tool life decreases with cutting speed. The relatively long life of the tools tested under cutting speeds close to 800 m/min verifies the speculation made in "Chip formation". The cutting speed of 800 m/min can be considered as a critical cutting speed. At this speed, relatively low mechanical load, relatively low degree of segmentation of the sawtooth chip, and relatively long tool life can be obtained.

The increasing trend of the tool life with cutting speed can be mainly attributed to the decreasing cutting force as shown in Fig. 2d. The decreasing degree of segmentation of

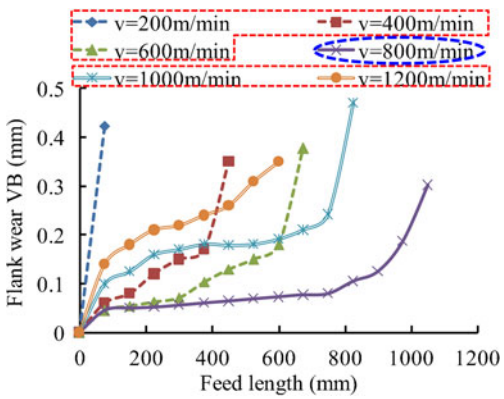

Fig. 10 Tool wear processes obtained under different cutting speeds (f_z=0.1 mm/tooth, a_p=0.3 mm)

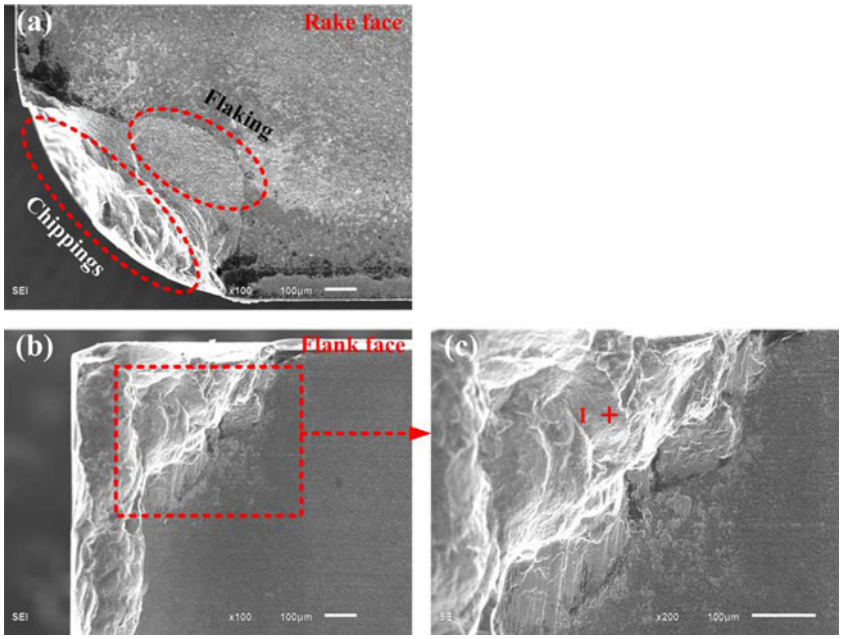

Fig. 11 **a**–**c** SEM images of the typical worn tool tested under cutting speed v=400 m/min (f_z=0.1 mm/tooth, a_p=0.3 mm)

sawtooth chip shown in Fig. 8 should also contribute to the increasing tool life to some extent. As for the decrease of tool life with cutting speed shown in Fig. 9, besides the influences of increasing cutting force and higher degree of sawtooth segmentation, the effect of much higher cutting temperature on tool wear should also be taken into account.

Figure 10 shows the tool wear evolutions obtained under different cutting speeds. It was found that there are apparent differences between the tools tested under cutting speeds below and above 800 m/min. When the cutting speed is below 800 m/min, the wear rate grows with the feed length and the tools are more likely to wear out in an abrupt way at the end of tool life. However, as the cutting speed increases over 800 m/min, though the wear rate is relatively high in the early and late stages of tool life, it is very small in the middle stage which account for the majority of tool life. For the cutting conditions under consideration, tool reliability should be higher when relatively high cutting speed is adopted. With the increase of cutting speed, thermal softening has a much greater effect on the reduction of the workpiece hardness than it does on that of tool material. Due to the greater gap of hardness, when the cutting speed is high, the wear rate is relatively small in the middle stage of tool life.

The analysis of tool life and tool wear process show that, for the tools tested in different cutting speed ranges (below and above 800 m/min), great differences exist. Taking the

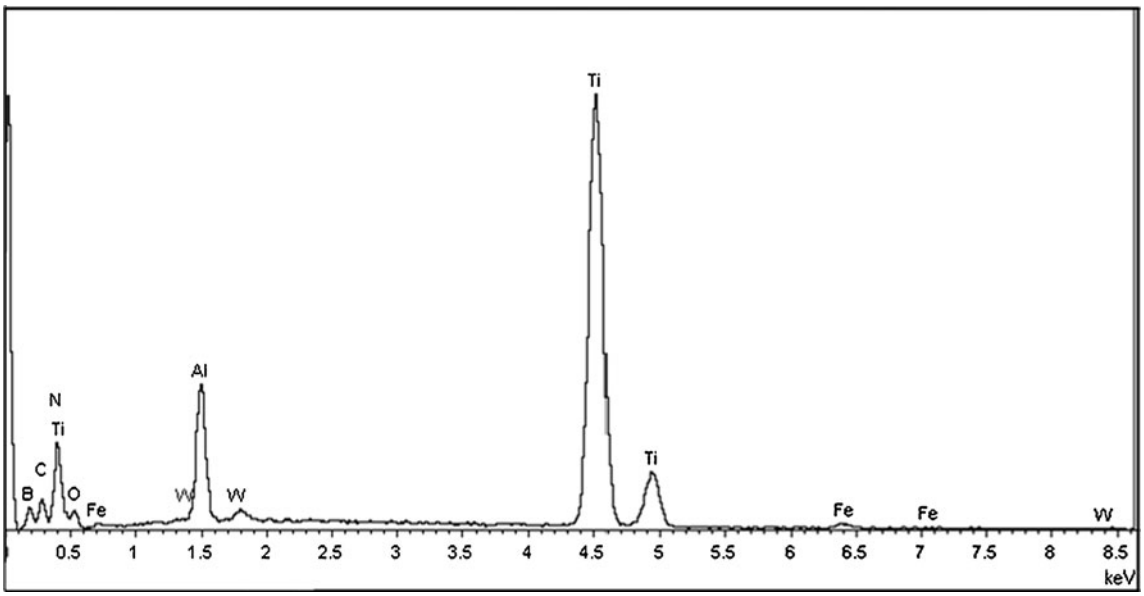

Fig. 12 EDS analysis of point 1 in Fig. 11c

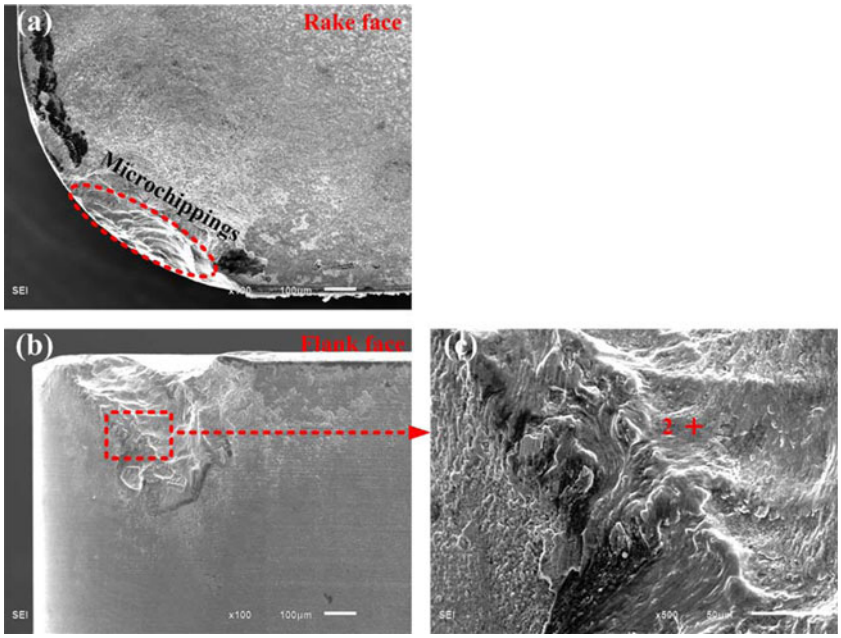

Fig. 13 **a**–**c** SEM images of the typical worn tool tested under cutting speed v=800 m/min (f_z=0.1 mm/tooth, a_p=0.3 mm)

critical cutting speed 800 m/min into consideration, the worn tools obtained under three cutting speeds (400, 800, and 1,200 m/min) are investigated in order to distinguish the characteristics of the tool wear mechanisms when tested in different cutting speed ranges.

Figure 11 shows the SEM images of the typical worn tool when the cutting speed of 400 m/min is adopted. It can be seen that a large flaked region appeared on the tool rake face. On the cutting edge, serious chippings happen. Since the cutting speed is relatively low, the effect of cutting temperature on tool wear is not obvious. It is inferred that the flaking and chippings are mainly caused by the relatively large mechnical load. The relatively large mechanical load as shown in Fig. 2d should also be the main reason for the catastrophic fracture which exists on the tool flank face. The relatively large mechanical and thermal impact that resulted from the high degree of segmentation of saw-tooth chip also contributed to these tool wear morphologies to some extent. Figure 12 shows the EDS analysis of point 1 denoted in Fig. 11c. The low content of element Fe (0.48 wt.%) and relatively low content of element O (7.98 wt.%) indicate that, due to the low cutting temperature, the effect of adhesive wear and oxidation wear on tool failure is relatively small.

As shown in Fig. 13, compared with the worn tools obtained under 400 m/min, no flaking occurred on the tool

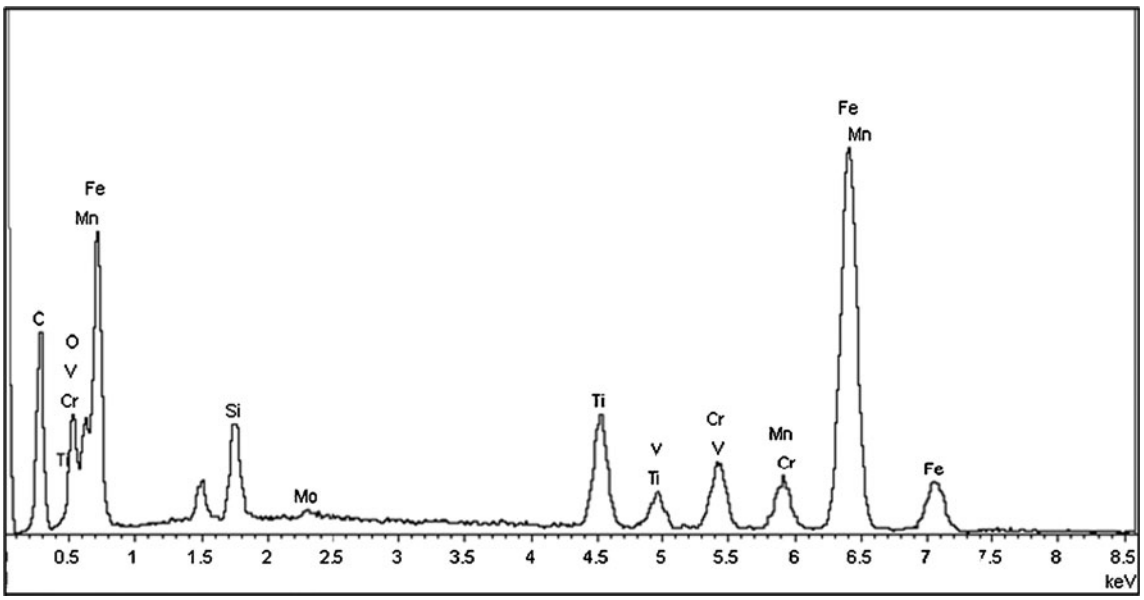

Fig. 14 EDS analysis of point 2 in Fig. 13c

rake face when the cutting speed was 800 m/min. There exist many microchippings on the cutting edge, and the worn region is much smaller. As for the flank face, the fractured region also becomes much smaller. These changes of tool wear morphologies should be attributed to the much lower mechanical load and much lower mechanical and thermal impact induced by low degree of segmentation of sawtooth chip. As the cutting speed increases, the influence of higher cutting temperature on tool wear become much more obvious. There seems to be serious adhesion on the tool flank face as shown in Fig. 13c. The EDS analysis of point 2 shown in Fig. 14 reveals that the content of element Fe and O is 35.8 and 13.16 wt.%, respectively, indicating the higher influence of adhesion and oxidation on tool flank wear.

Maily due to the effect of much higher cutting temperature, the tool wear mechanisms of the tools tested under the cutting speed of 1,200 m/min are very different from those obtained using a relatively low cutting speed. Liquid-like materials appear on the rake face of the cutting tool as shown in Fig. 15a. It was found that there were many gas cavities in them. The EDS analysis of point 3 denoted in Fig. 15a reveals elements from the workpiece material and element O as shown in Fig. 16a. The content of element Fe and O is 49.98 and 37.36 wt.%, respectively. It is inferred that the liquid-like materials are the

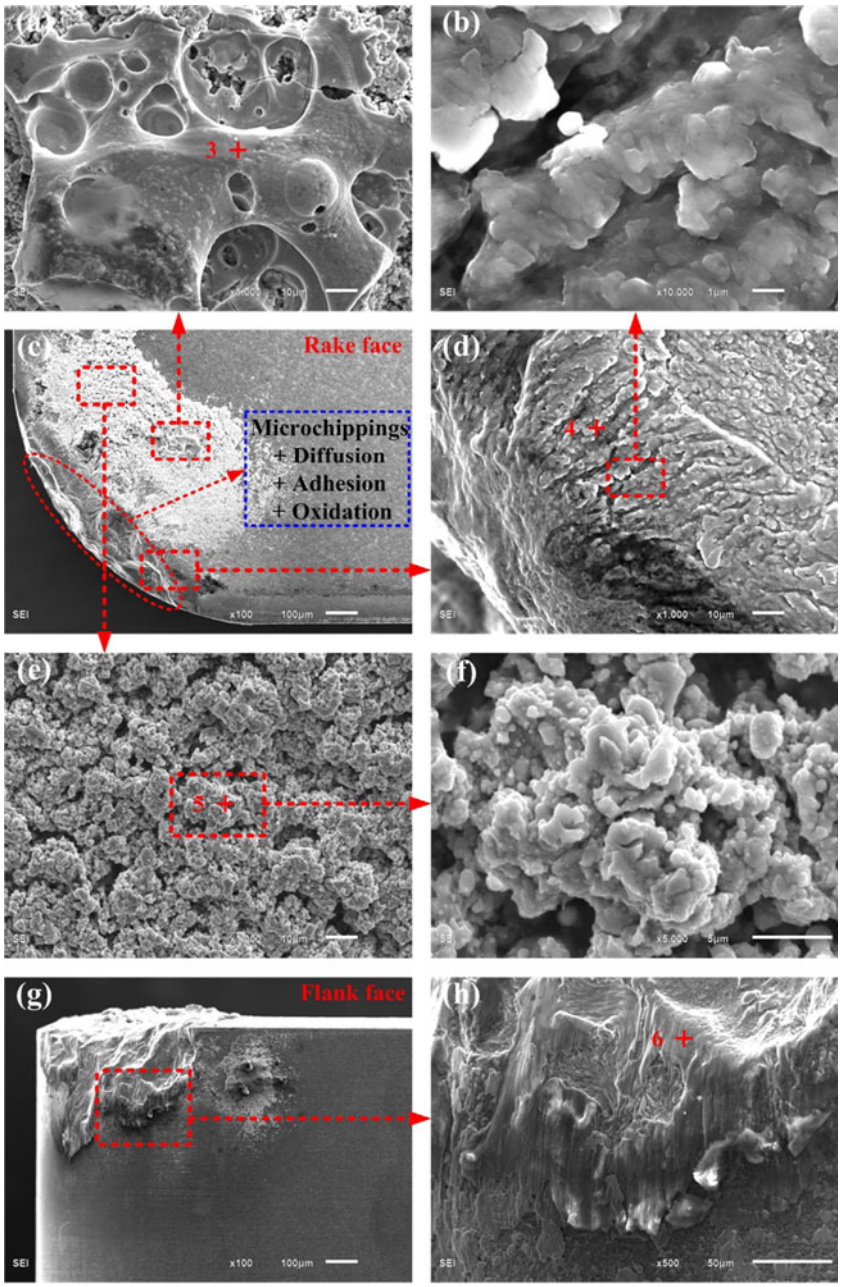

Fig. 15 **a**–**h** SEM images of the typical worn tool tested under cutting speed v=1,200 m/min (f_z=0.1 mm/tooth, a_p=0.3 mm)

melt chip, which is the product that resulted from the fierce physical and chemical reactions between the workpiece material and the atmosphere under high cutting temperature. Taking the melt point of the workpiece material into consideration, in some local region the cutting temperature should be more than 1,427 °C.

There are many particulates distributed on the tool rake face as shown in Fig. 15e, f. As the distribution of these particulates shows no direction, they should not be caused by the adhesion from the workpice material. Figure 16c shows the EDS analysis of point 5 in Fig. 15e. A large content of element Fe (77.72 wt.%) and element O (7.95 wt.%), respectively, indicates that they are the workpiece material which has reacted with oxygen. As shown in Fig. 17, during the milling process, the chip flew away with very high temperature. Some of these chips were melt as shown in Fig. 15a. The temperature of the melt chip surface decreased rapidly when it was flying away, and slag

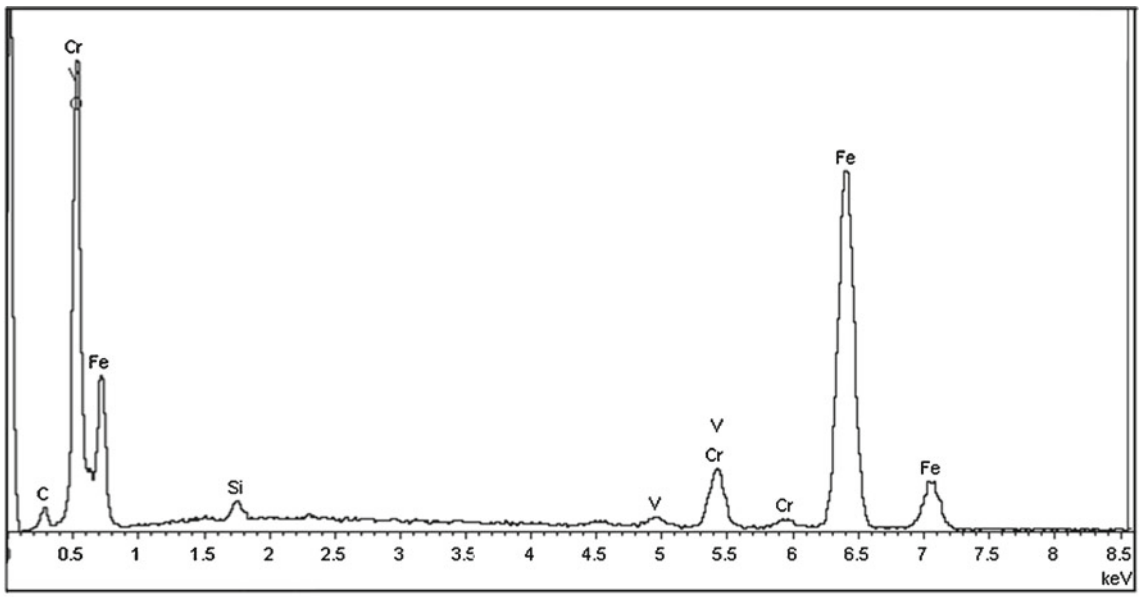

(a) EDS analysis of point 3 in Fig. 15 (a).

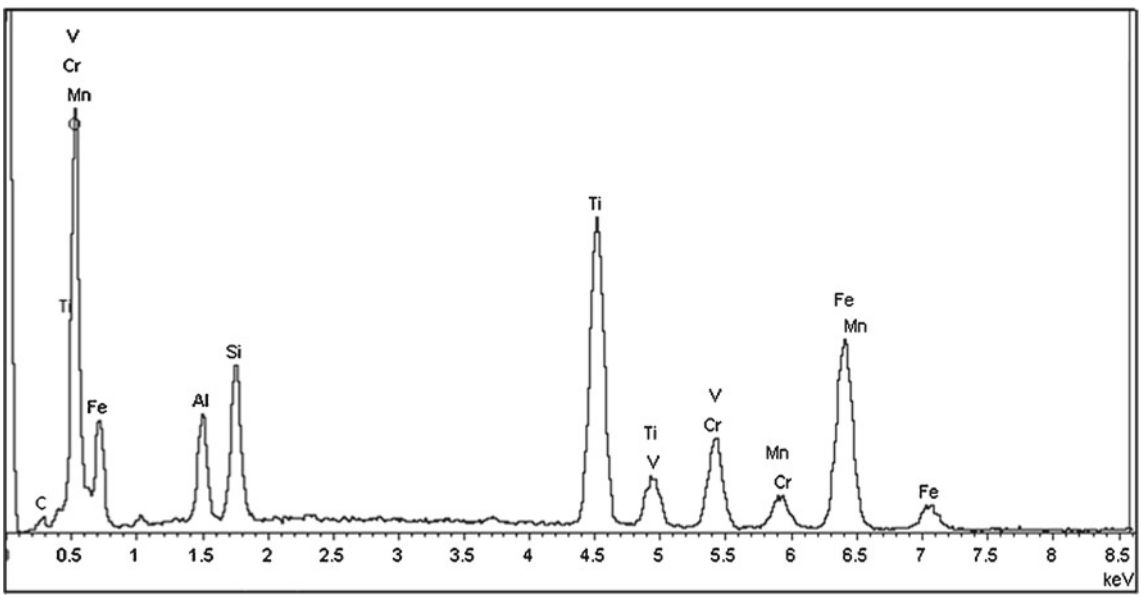

(b) EDS analysis of point 4 in Fig. 15 (d).

Fig. 16 EDS analyses of points 3, 4, 5, and 6 in Fig. 14b. **a** EDS analysis of point 3 in Fig. 15a. **b** EDS analysis of point 4 in Fig. 15d. **c** EDS analysis of point 5 in Fig. 15e. **d** EDS analysis of point 6 in Fig. 15h

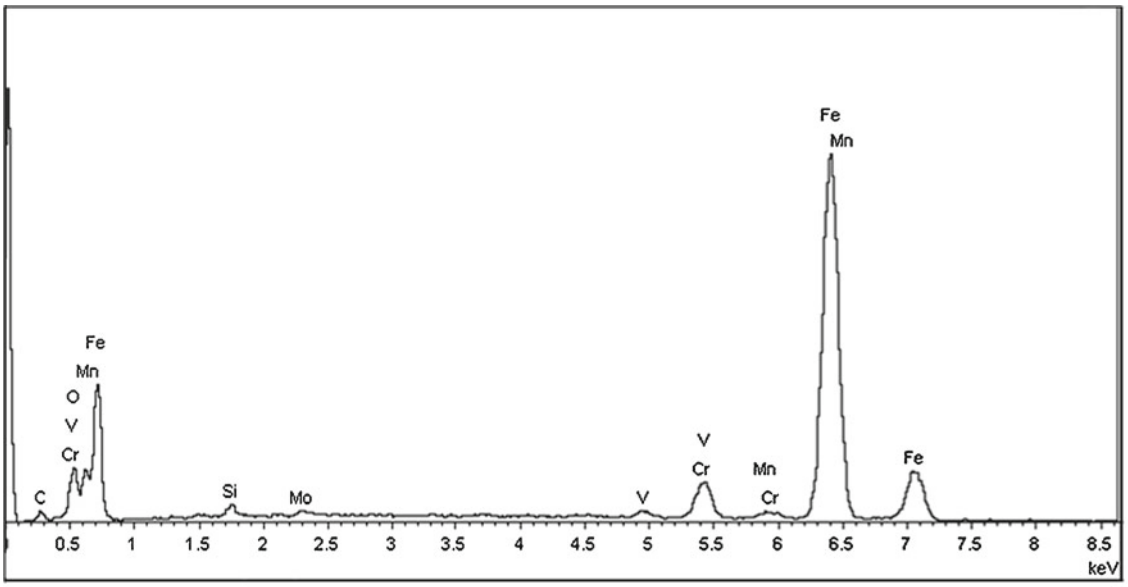

(c) EDS analysis of point 5 in Fig. 15 (e).

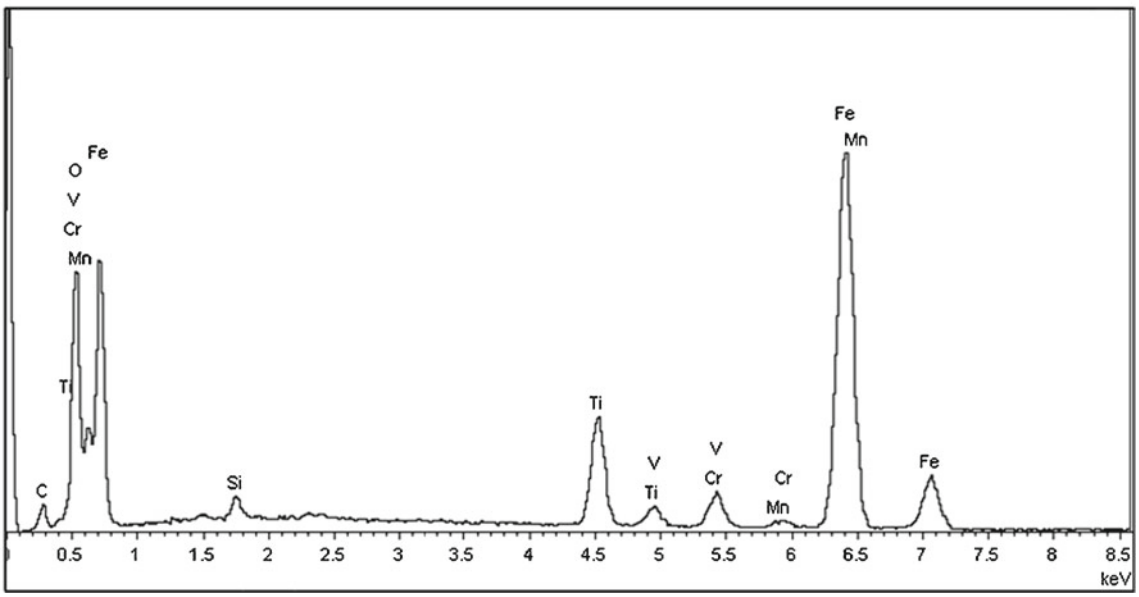

(d) EDS analysis of point 6 in Fig. 15 (h).

Fig. 16 (continued)

probably formed on the chip surface. Due to the interaction between the chip and the cutting tool, particulates from the chip surface landed on the tool rake face. The accumulation of these particulates on the tool rake face formed the morphologies shown in Fig. 15e, f.

Compared with the tools tested under 800 m/min, the region of the worn cutting edge seems to be smaller and smoother when the cutting speed is 1,200 m/min. As the cutting speed increases, it seems that the region of the cutting edge is becoming smaller, which can be attributed to the shorter tool–chip contact length caused by higher cutting cutting speed. As stated by Molinari and Nouari [24], diffusion at the tool–chip interface is controlled by the contact temperature, and diffusion wear is characterized by a smooth worn surface with no plastic deformation. The smoother worn cutting edge can be attributed to diffusion wear accelerated by high cutting temperature. The EDS analysis of point 4 in

Fig. 17 Photo captured during the milling process (v=1,200 m/min, f_z=0.1 mm/tooth, a_p=0.3 mm)

Fig. 15d shows a large amount of element Fe and O (17.76 and 45.59 wt.%, respectively), indicating the great effect of adhesion and oxidation on the wear of cutting edge. From Fig. 15d, it can be seen that there are many grooves perpendicular to the cutting edge, which is not encountered when the cutting speed is 800 m/min. The magnified image in Fig. 15e shows that there are microcracks located at the bottom of these grooves. Taking the directions of these grooves into consideration, it seems that besides microchipping, diffusion, adhesion, and oxidation, thermal crack caused by high temperature gradient also contributes greatly to the failure of the cutting edge.

Serious adhesion appears on the tool flank face when the cutting speed is 1,200 m/min as shown in Fig. 15g, h. The high cutting temperautre has great influence on the formation of larger amounts of adhesion. The EDS analysis of point 6 denoted in Fig. 15h is shown in Fig. 16d. It was found that there is a high content of elements Fe and O (50.69 and 30.32 wt.%, respectively) in the adhesive region, meaning that, besides fracture, adhesion and oxidation also influence the flank wear greatly.

By means of comparing the tool mechanisms under different cutting speeds, it can be concluded that, as the cutting speed increases, the influences of fracture and chipping that resulted from mechanical load on tool wear are reduced, while the influences of adhesion, oxidation, and thermal crack accelerated by high cutting temperature become greater. At the cutting speed of 800 m/min, both the influences of mechanical load and cutting temperature on tool wear are relatively low, and relatively long tool life can be obtained at this critical cutting speed.

4 Conclusions

High-speed face milling experiments of AISI H13 steel (46–47 HRC) were conducted with CBN tools used. High cutting speeds ranging from 200 to 1,200 m/min were adopted. This paper focused on the velocity effects on cutting forces, chip formation, and tool wear. Their evolutions with cutting speed were identified and analyzed. The characteristics of wear mechanisms of tools tested under different cutting speeds were investigated and compared. The following conclusions can be made:

- As the cutting speed increases, the cutting forces F_{sx}, F_{sy}, and F_{sz} decrease firstly and then increase with the cutting speed, and they reach valley values at cutting speeds of 600, 700, and 800 m/min, respectively. As for the resultant cutting force F_{sr}, it evolves in a similar way and the smallest value arises when the cutting speed is 800 m/min. The decreasing trend of cutting forces is mainly caused by the combined effects of the influencing factors such as reduction of the shear strength in the shear zone, chip thickness, tool–chip contact area, and increase of shear angle, all of which resulted from higher cutting speed, while the increasing trend can be mainly attributed to the increase of tool wear. When the cutting speed is above 800 m/min, the influence of feed per tooth and depth of cut on F_{sr} increases and decreases, respectively.
- As the cutting speed increases, the shape of the chip evolves in the following order: long helix chip (v= 200 m/min), washer-shaped chip (v=400 m/min), short arc-shaped chip (v=600 m/min, v=800 m/min), and long helix chip (v=1000 m/min, v=1200 m/min). Chip breaking seems to be more likely to happen when the cutting speed is between 600 and 800 m/min. The degree of chip segmentation decreases firstly with cutting speed and arrives at a valley value at the cutting speed of 800 m/min. Then, it increases with the cutting speed. The development of chip segmentations can be attributed to the evolution of strain rate and cutting temperature with cutting speed.
- Compared with the variation trend of cutting forces and chip formation, the tool life evolves in an opposite way; namely, it initially increases with the cutting speed and then decreases. The opposite trend of the tool life with cutting speed reveals the correlations among cutting forces, chip formation, and tool wear and verifies the speculation that, at the cutting speed of 800 m/min, relatively long tool life can be obtained. By comparing the evolution process of tool wear with cutting speed in different speed ranges, it was found that higher tool reliability is expected to arise when the cutting speed is above 800 m/min. When the cutting speed increases, the influences of fracture and chipping caused by mechanical load on tool wear are reduced, while the influences of adhesion, oxidation, and thermal crack

accelerated by high cutting temperature become greater. At the critical cutting speed of 800 m/min, due to the relatively low influences of mechanical load and cutting temperature on tool wear, relatively long tool life can be obtained.

Acknowledgments This research is supported by the National Basic Research Program of China (2009CB724402), the National Natural Science Foundation of China (51175310), and the Graduate Independent Innovation Foundation of Shandong University, GIIFSDU (yzc10119).

References

1. Trent EM, Wright PK (2000) Metal cutting, 4th edn. Butterworth-Heinemann, Woburn
2. Huang Y, Liang SY (2003) Cutting forces modeling considering the effect of tool thermal property—application to CBN hard turning. Int J Mach Tools Manuf 43(3):307–315
3. Huang Y, Liang SY (2005) Modeling of cutting forces under hard turning conditions considering tool wear effect. J Manuf Sci Eng Trans ASME 127(2):262–270
4. Benga GC, Abrao AM (2003) Turning of hardened 100Cr6 bearing steel with ceramic and PCBN cutting tools. J Mater Process Technol 143–144(1):237–241
5. El-Wardany TI, Kishawy HA, Elbestawi MA (2000) Surface integrity of die material in high speed hard machining. Part 1: micrographical analysis. J Manuf Sci Eng Trans ASME 122:620–631
6. Özel T, Hsu TK, Zeren E (2005) Effects of cutting edge geometry, workpiece hardness, feed rate and cutting speed on surface roughness and forces in finish turning of hardened AISI H13 steel. Int J Adv Manuf Technol 25:262–269
7. Chen W (2000) Cutting forces and surface finish when machining medium hardness steel using CBN tools. Int J Mach Tools Manuf 40:455–466
8. Arsecularatne JA, Zhang LC, Montross C, Mathew P (2006) On machining of hardened AISI D2 steel with PCBN tools. J Mater Process Technol 171:244–252
9. Dawson T (2002) Machining hardened steel with polycrystalline cubic boron nitride cutting tools. Ph.D. thesis, Georgia Institute of Technology, Atlanta
10. Huang Y (2002) Predictive modeling of tool wear rate with application to CBN hard turning. Ph.D. thesis, Georgia Institute of Technology, Atlanta
11. Barry J, Byrne G (2001) Cutting tool wear in the machining of hardened steels: part II: cubic boron nitride cutting tool wear. Wear 247:152–160
12. Poulachon G, Moisan A, Jawahir IS (2001) Tool-wear mechanisms in hard turning with polycrystalline cubic boron nitride tools. Wear 250:576–586
13. Chou YK, Evans CJ, Barash MM (2002) Experimental investigation on CBN turning of hardened AISI 52100 steel. J Mater Process Technol 124:274–283
14. Huang Y, Liang SY (2004) Modeling of CBN tool flank wear progression in finish hard turning. J Manuf Sci Eng Trans ASME 126(1):98–106
15. Huang Y, Liang SY (2004) Modelling of CBN tool crater wear in finish hard turning. Int J Adv Manuf Technol 24(9–10):632–639
16. Aslan E (2005) Experimental investigation of cutting tool performance in high speed cutting of hardened X210 Cr12 cold-work tool steel (62 HRC). Mater Des 26:21–27
17. Koshy P, Dewes RC, Aspinwall DK (2002) High speed end milling of hardened AISI D2 tool steel (58 HRC). J Mater Process Technol 127:266–273
18. Braghini A, Coelho RT (2001) An investigation of the wear mechanisms of polycrystalline cubic boron nitride (PCBN) tools when end milling hardened steels at low/medium cutting speeds. Int J Adv Manuf Technol 17:244–251
19. Okada M, Hosokawa A, Tanaka R, Ueda T (2011) Cutting performance of PVD-coated carbide and CBN tools in hardmilling. Int J Mach Tools Manuf 51:127–132
20. Dimla DE, Lister PM (2000) On-line metal cutting tool condition monitoring. I: force and vibration analysis. Int J Mach Tools Manuf 40(5):739–768
21. Shaw MC (1997) Metal cutting principles. Clarendon, Oxford
22. Ai X (2003) High speed machining technology. National Defense Industry, Beijing
23. Oxley PLB (1989) Mechanics of machining. Horwood, Chichester
24. Molinari A, Nouari M (2002) Modeling of tool wear by diffusion in metal cutting. Wear 252:135–149